Impact of aircraft emissions on reactive nitrogen over the North Atlantic Flight Corridor region

M. Koike,[1] Y. Kondo,[1] H. Ikeda,[1] G.L. Gregory,[2] B.E. Anderson, [2] G.W. Sachse,[2] D. Blake,[3] S.C. Liu,[4] H.B. Singh,[5] A. Thompson, [6] K. Kita,[7] Y. Zhao,[1] T. Sugita,[8] R.E. Shetter,[9] and N. Toriyama[1]

[1] Solar-Terrestrial Environment Laboratory, Nagoya University, Toyokawa, Japan.
[2] NASA Langley Research Center, Hampton, VA
[3] University California, Irvine, CA
[4] Georgia Institute of Technology, Atlanta, GA
[5] NASA Ames Research Center, Moffett Field, CA
[6] NASA Goddard Space Flight Center, Greenbelt, MD
[7] Department of Earth and Planetary Physics, Graduate School of Science, University of Tokyo, Tokyo, Japan
[8] National Institute for Environmental Studies, Onogawa, Tsukuba, Japan.
[9] Atmospheric Chemistry Division, National Center for Atmospheric Research, Boulder, CO

IN PRESS

Short title: AIRCRAFT IMPACT ON NO_y
Submitted to the Journal of Geophysical Research
August 16, 1999

Abstract. The impact of aircraft emissions on reactive nitrogen in the upper troposphere (UT) and lowermost stratosphere (LS) was estimated using the NO_y-O_3 correlation obtained during the SASS Ozone and NO_x Experiment (SONEX) carried out over the US continent and North Atlantic Flight Corridor (NAFC) region in October and November 1997. To evaluate the large scale impact, we made a reference NO_y-O_3 relationship in air masses, upon which aircraft emissions were considered to have little impact. For this purpose, the integrated input of NO_x from aircraft into an air mass along a 10-d back trajectory (ΔNO_y) was calculated based on the ANCAT/EC2 emission inventory. The excess NO_y (dNO_y) was calculated from the observed NO_y and the reference NO_y-O_3 relationship. As a result, a weak positive correlation was found between the dNO_y and ΔNO_y, and dNO_y and NO_x/NO_y values, while no positive correlation between the dNO_y and CO values was found, suggesting that dNO_y values can be used as a measure of the NO_x input from aircraft emissions. The excess NO_y values calculated from another NO_y-O_3 reference relationship made using in-situ CN data also agreed with these dNO_y values, within the uncertainties. At the NAFC region (45°N – 60°N), the median value of dNO_y in the troposphere increased with altitude above 9 km and reached 70 pptv (20 % of NO_y) at 11 km. The excess NO_x was estimated to be about half of the dNO_y values, corresponding to 30 % of the observed NO_x level. Higher dNO_y values were generally found in air masses where O_3 = 75 – 125 ppbv, suggesting a more pronounced effect around the tropopause. The median value of dNO_y in the stratosphere at the NAFC region at 8.5 – 11.5 km was about 120 pptv. The higher dNO_y values in the LS were probably due to the accumulated effect of aircraft emissions, given the long residence time of affected air in the LS. Similar dNO_y values were also obtained in air masses sampled over the US continent.

1. Introduction

Nitrogen oxide radicals ($NOx = NO + NO_2$) play a critical role in the photochemistry of ozone (O_3) and hydrogen oxide radicals ($HOx = OH$ + peroxy radicals) in the upper troposphere (UT) and lowermost stratosphere (LS). The major sources of total reactive nitrogen ($NO_y = NO + NO_2 + NO_3 + HNO_2 + HNO_3 + HNO_4 + 2N_2O_5$ + PAN + other organic nitrates + aerosol nitrates) in the UT are transport from the stratosphere, NO production by lightning, aircraft NO_x emissions, and convective transport of NO_y rich air from the continental surface where NO_x is produced by fossil fuel combustion and other processes. According to 3-D model calculations, the contribution from each source is similar in magnitude at northern midlatitude UT during winter, while lightning becomes a major source in summer [Lamarque et al., 1996]. Because of a rapid growth in air traffic in recent years, greater attention has been paid to the impact of aircraft NO_x emissions on the O_3 chemistry in the UT and LS. Model calculations predict that aircraft emissions can have significant impact on large scale NO_x distributions in the UT and LS in the northern midlatitudes and high latitudes [*Brasseur et al.*, 1996]. The emissions are especially extensive in the North Atlantic Flight Corridor (NAFC) region, where commercial air traffic is heavy at altitudes between 10 and 12 km [*Baughcum et al.*, 1996; *Gardner*, 1998]. The maximum increase in NO_x in the NAFC region was estimated to be between 50 and 90 parts per trillion (pptv) at 200 hPa for July, based on several 3-D model calculations using a 1990 fleet of subsonic aircraft [*Brasseur et al.*, 1996, 1998 and references therein]. Sharp increases in NO_x concentrations within aircraft contrails were observed in the eastern NAFC region and an aircraft source was successfully identified in some cases [*Schlager et al.*, 1997; *Klemm et al.*, 1998]. Although the large-scale effect (e.g. corridor effect) from aircraft emissions is more difficult to evaluate from the observation, a regional scale enhancement in NO/NO_y ratio was identified in the LS over the east coast of the US continent by comparing the observed ratios with those of trajectory model calculations [*Witte et al.*, 1997].

The Subsonic ASSessment (SASS) Ozone and NOx experiment (SONEX) was carried out using NASA's DC-8 aircraft in October and November 1997. Most of the aircraft measurements were

made over the US continent and the NAFC region (Figure 1). Four intensive flights were made from both Bangor, Maine (45°N, 68°W) and Shannon, Ireland (53°N, 9°W). A substantial amount of the data was obtained at altitudes between 8 and 11.5 km in both the UT and LS. Details of the experiment are described by *Singh et al.* [1999].

In this paper, the impact of aircraft emissions on amount of reactive nitrogen was estimated using the NO_y - O_3 correlation. This is because a positive correlation between NO_y and O_3 was generally observed in the UT and LS [*Murphy et al.*, 1993; *Ridley et al.*, 1994; *Kondo et al.*, 1996] and the aircraft emissions can alter their correlation [*Koike et al.*, 1997]. In Plate 1, a correlation plot between NO_y and O_3 using all of the 10-s SONEX data obtained above 8.5 km are shown. In this plate, we excluded the data obtained within aircraft plumes, influenced by lightning, or affected by recent convective transport, as described in detail in the following section. As seen in this plate, the NO_y values at 45°N – 60°N and those over the US continent are generally higher than those obtained over the west coast of the US and at 30°N-45°N and 60°N-70°N, where air traffic density is lower. As described in the following sections, a reference NO_y - O_3 relationship will be derived using data from air masses, in which aircraft emissions are considered to have little impact, i.e. "background air". The excess NO_y (dNO_y) will be estimated using this reference relationship. The statistical analyses of these dNO_y values will be made for the data obtained at 45°N – 60°N over the Atlantic (corresponding to the NAFC) and the US continent. The exess NO_x (dNO_x) will also be estimated using the reference NO_x/NO_y ratio in the background air.

2. Measurements and Data

2.1. Measurements

The NO and NO_y instrument used for SONEX was very similar to that used during NASA's Pacific Exploratory Mission West-B (PEM-W-B) conducted in 1994 [*Kondo et al.*, 1997]. Both NO and NO_y were measured using a chemiluminescence technique. NO_y compounds were catalytically converted into NO on the surface of a heated gold tube with the addition of CO. The inlet tube for air sampling faced rearward discriminating against particles of diameter larger than about 1 μm. The data were recorded every 1-s, however, 10-s averaged data were used in this study. The precision of the 10-s NO and NOy measurements at 10 km estimated from the photon counts fluctuations (2σ) was 6 and 19 pptv for the NO and NO_y values of 100 and 800 pptv, respectively. The absolute accuracy was estimated to be 8 and 10 % for these NO and NO_y values.

During the SONEX project the same gold tube was used for all NO_y measurements. Other than operating the instrument using synthetic air, no attempt was made to clean the tube. The conversion efficiency of NO_2 in ambient air was 99±1 % during each flight. Possible interference in the NO_y measurements from the conversion of HCN, NH_3, and CH_3CN was checked in the laboratory and during the flights. The conversion efficiency of HCN in dry synthetic air was between 0.5 and 4 % on the ground before, during, and after the mission. It was also measured during the two test flights (at 6.4–11.9 km), using two independent NO_y channels and by adding a known amount of HCN gas into one of the channels. For one flight, the conversion efficiency was 2.1±0.5 % for the O_3 and H_2O mixing ratios of 62-140 parts per billion (ppbv) and 23-235 parts per million (ppmv), respectively. For the other flight it was 1.6±0.5 %, although the O_3 and H_2O values were not measured. From these results, HCN was estimated to have contributed about 4 pptv to the SONEX NO_y data assuming an average HCN mixing ratio of about 200 pptv [*Rinsland et al.*, 1982; *Mahieu et al.*, 1995]. The conversion efficiencies of NH_3 and CH_3CN were also measured in the laboratory at 1-3 and 0.5-2 %, respectively. Assuming mixing ratios of NH_3 and CH_3CN in the UT of 1 pptv [*Ziereis and Arnold*, 1986] and 200 pptv [*Hamm et al.*, 1989], the interference from these species is

considered to be negligible.

During the SONEX experiment, the actinic flux was measured using grating monochromators to calculate photolysis rate of NO_2 ($J(NO_2)$) [*Shetter and Müller,* 1999]. The photostationary state NO_2/NO ratios were calculated using the measured values of O_3, temperature, pressure, and $J(NO_2)$ for periods when the solar zenith angles were lower than 87°. The NO_x mixing ratios were calculated from these NO_2/NO ratios and the observed NO mixing ratios. The calculated NO_2/NO ratios and NO_x values were compared with those calculated using a box model in which a more complete photochemistry was included [*Jaegle et al.*, 1998]. As a result, they agreed within 30 % and 10 %, respectively, at altitudes above 7 km. Simplified chemistry was used in this study to maximize the amount of NO_x data.

In this study, 10-s averaged data of O_3, N_2O, and CO were also used. The O_3 measurements were made using a chemiluminescence technique, and N_2O and CO were measured using a tunable diode laser system. The concentration of condensation nuclei (CN) with a diameter larger than 15 nm (CN fine particle; TSI model 3760) [*Anderson et al.*, 1999] was also used in this study. The unit of CN concentration was normalized to 0°C temperature and 1013 hPa (STP-cm^3) to represent the CN mixing ratio. Nonmethane hydrocarbons (NMHCs) and halocarbons were measured by collecting whole air samples and analyzing them using gas chromatography and flame ionization and electron capture detectors. The detection limit and sampling frequency of these measurements are summarized by *Singh et al.* [1999] and *Simpson et al.* [1999].

2.2. Data Selection

During the SONEX experiment, most of the data were obtained at altitudes between 8 and 11.5 km. Air masses with O_3 values lower and higher than 100 ppbv were defined as tropospheric and stratospheric, respectively. The stratospheric air masses were sampled at potential temperatures between 310 and 360 K, within the lowermost stratosphere (LS), the region above the midlatitude tropopause and below the isentrope touching the tropical tropopause, roughly 385 K, defined by *Holton et al.* [1995]. Based on the Microwave Temperature Profiler (MTP) tropopause height data,

the LS data were obtained within 2 km from the tropopause. The MTP data also showed that air masses with O_3 values higher than 100 ppbv were sometimes obtained below the tropopause even though a clear signature of stratospheric air intrusion was not seen in the airborne DIfferential Absorption Lidar (DIAL) O_3 data. However in general, air masses with O_3 values higher than 100 ppbv were considered to have the same chemical characteristics as those from the LS. Similarly, air masses in which O_3 values lower than 100 ppbv observed above the MTP derived tropopause height were regarded as the UT ones.

In the present study, an increase in NO_x and NO_y from aircraft emissions was estimated for two study areas. The first area chosen was at latitudes between 45°N and 60°N and at longitudes between 0°W and 80°W. This data set was obtained mostly during the intensive flights from Bangor and Shannon (Figure 1). Air traffic density is quite high in this area and will be referred to as the "NAFC region" in the following. The other area was located over the US continent at latitudes between 35°N and 45°N and at longitudes between 70°W and 120°W. The data set in this area was obtained during the two transit flights made on October 13, 1997 (971013) and 971112 between NASA Ames on the US west coast and Bangor on the east coast. This area will be referred to as the "US continent region".

When the measurements were made within the heavy air traffic region, sharp simultaneous increases in NO and NO_y values were often seen [*Sugita et al.*, 1999; *Anderson et al.*, 1999]. These air masses were most likely sampled within aircraft plumes. The increase in the 1-s NO and NO_y data ranged from 100 pptv to a few ppbv. The time duration of the enhancement ranged from 1-s to 60-s, with a median value of 4-s. Given the typical cruise speed of the NASA DC-8 aircraft of 200-250 m/s, the horizontal scales of the plumes were smaller than about 10 km with a typical size of about 1 km. Based on the Gaussian plume model, aircraft emission plumes are diluted to background concentrations within 5 to 10 hours for a typical wind shear condition with a corresponding horizontal size of 20 km [*Schlager et al.*, 1997; *Gerz et al.*, 1998]. Although the size of the NO_y enhancement observed from the NASA DC-8 depends on the geometry of the plume crossing, the maximum size of the observed plume was comparable to these estimates. These estimates were also

consistent with a plume age of 10 minutes to 10 hours estimated using peak NO_y mixing ratios observed during SONEX [*Anderson et al.*, 1999]. In this study, the data obtained within the plumes were excluded in the evaluation of the large scale impact from the aircraft emissions. This was because the sampling frequency of the plumes depends on the location and time of the measurement (many plumes were observed when the measurements were made in air masses just after heavy air traffic had finished) and an inclusion of these data could be a potential cause of a bias in estimating the aircraft impact. The excluded data corresponded to 6 % of the entire data set at the 8.5 to 11.5 km altitude range. Because they were relatively small amount, the results of this study would not change significantly even the plumes were included in the analyses.

A clear signature of NO production by lightning was seen during four flights, on 971013, 971029, 971103, and 971109 [*Thompson et al.*, 1999; *Pickering et al.*, 1999]. In these cases the NO_x and NO_y mixing ratios increased more than 1 ppbv and NO_x/NO_y ratios ranged between 0.4 and 1.0 suggesting that NO production by lightning had occurred within a few days prior to the measurements. These results were generally consistent with the analyses of the air mass trajectories, convective activities using cloud images, and lightning activities detected by the US ground based lightning network [*Thompson et al.*, 1999; *Pickering et al.*, 1999]. Possible influences from the lightning were also observed on 971020 and 971028. In this study, all of the data likely to have been influenced by NO production by lightning were excluded. It should be noted, however, that the influence of lightning cannot be identified in an air mass, once the NO_x in the air mass is diluted down near the background level. Consequently we could not completely remove from our analysis the data which might have been affected by NO production from lightning. The contribution from lighting will be revisited in Section 3.2.3.

The vertical profile of the CO in the troposphere is shown in Figure 2 using all of the data except for those obtained from aircraft plumes and clearly influenced by lightning. The median values and 67 % ranges in the NAFC region are also shown. As seen in this figure, the CO mixing ratio generally decreased with altitude and the median values were between 76 and 82 ppbv at 9 to 11 km. These values were systematically lower than the median CO values of 100 to 105 ppbv

obtained in the continental or maritime air masses in the UT over the middle to high latitude western Pacific in September and October [*Kondo et al.*, 1996]. In Figure 3, a correlation plot between NO_y and CO is shown using the data obtained at altitudes above 8.5 km. Different symbols are used for the UT and LS data. The NO_y mixing ratio did not generally have a positive correlation with the CO mixing ratio in the UT. These results suggest that NO_y values in most of air masses in the UT obtained during SONEX had not been influenced by recent convective transport of polluted continental surface air. To eliminate the possible influence from recent convection, the data with CO values higher than 100 ppbv was excluded in this study. In addition, data showing a clear positive correlation between CO and NO_y, were also excluded. The excluded data by these criteria corresponded to 19 % of the entire UT data set obtained above 8.5 km.

The correlations of NO_y with nonmethane hydrocarbons such as ethyne (C_2H_2), ethane (C_2H_6), and propane (C_3H_8), and halocarbons such as perchloroethene (C_2Cl_4), methyl iodide (CH_3I), and $CHBr_3$ were also examined. No clear positive correlation was seen in the UT. In fact, NO_y decreased with increasing mixing ratios of these hydrocarbons and halocarbons for NO_y mixing ratios higher than 300 pptv (not shown). C_2H_2, C_2H_6, C_3H_8, and C_2Cl_4 are emitted in urban areas. CH_3I and $CHBr_3$ are considered to be good indicators of maritime air mass. The photochemical lifetimes of these species are comparable or shorter than that of CO. Consequently, the lack of a clear correlation of NO_y with these species further confirms that the data selected in this study were generally free from the recent convective transport of air influenced by urban and other surface sources.

3. Results and Discussion

3.1. Reference NO_y-O_3 Relationship

To estimate the increase in the NO_y mixing ratio due to aircraft emissions, we utilized a method that uses the NO_y-O_3 relationship. In this method, a reference NO_y-O_3 relationship was estimated using data in air masses upon which aircraft emissions were believed to have had little impact, i.e. "background air masses". To select the background air masses at 8.5-11.5 km, two independent approaches were taken. As described below, the agreement in the estimates on the excess NO_y derived from these two approaches was evaluated and the first approach described below was used for the further analyses.

For the first approach, 10-d back trajectories were calculated using a kinematic method for air masses sampled every 1 minute on board the NASA DC-8. The European Center for Medium-Range Weather Forecasts (ECMWF) data were used for this calculation. Then an integrated value of expected NO_x input from the aircraft emissions along each trajectory was calculated using the monthly mean values of the three dimensional NO_x emission distribution for October 1992, compiled in the ANCAT/EC2 emissions inventory [*Gardner*, 1998]. No chemical loss or diffusion process and no diurnal variation in NO_x emission rate was taken into account for this calculation, although some initial dilution effect was included because the emission rate was provided for each 1°×1° in latitude and longitude and every 1 km in altitude. The typical emission rate in the corridor region was 2-5 pptv hour^{-1}. The calculated value is denoted as ΔNO_y. For the present analysis, air masses in which the ΔNO_y value was less than 40 pptv were used for the reference relationship irrespective of the location in which they were sampled. A large portion of the data in the O_3 = 100–200 ppbv range was obtained off the west coast of the US (flight on 971009). These air masses had been transported by westerly winds from locations over the Pacific ocean where aircraft emissions are climatologically not very high. The data obtained at latitudes lower than 45°N and higher than 60°N was also selected as background for both the UT and LS. The criterion of 40 pptv within 10-d used in this study was admittedly arbitrary and subjective. A value of 40 pptv was

chosen simply because enough data points in each O_3 range were selected by this criterion. However, the resultant estimates of aircraft effects were not very sensitive to the choice of this criterion as long as it was relatively small. If real background air masses were based on the criterion of ΔNO_y = 0 pptv, the data selected under the present criterion would underestimate the aircraft impact. When 40 pptv was chosen as the criterion, 42 and 37 % of the UT and LS air masses sampled above 8.5km were classified as background air masses. In air masses when the ΔNO_y values were lower or higher than 40 pptv, the median ΔNO_y value was 17 or 100 pptv, respectively, in the UT, suggesting a large difference in the effect of aircraft on the two sets of air masses. The same feature was also seen in the LS where the median value of ΔNO_y was 14 and 107 pptv. The median value of the NO_y mixing ratio in the background air mass was then calculated for each 10 ppbv O_3 range and a linear relationship was calculated using these median values in the UT and LS separately as shown in Figure 4. The relationships in the UT and LS were smoothly connected at the O_3 value of 100 ppbv. Using the reference NO_y-O_3 relationship (referred as the "low ΔNO_y reference" hereafter), the expected NO_y value in the background air mass was calculated using the O_3 value simultaneously observed. The difference between this expected NO_y value and the observed NO_y value was defined as an excess NO_y (dNO_y).

For the second approach, the CN concentration was chosen as the criterion. This is because within the plume of the aircraft, enhancements of the CN value were often observed simultaneously with enhancements of the NO and NO_y [*Anderson et al.*, 1999]. Consequently, relatively higher CN values can be expected when an air mass is influenced by aircraft emissions. As shown in Figure 5, the CN concentration increased with altitude both in the UT and LS. These vertical profiles could partly be due to aircraft emissions which are most intensive at altitudes between 10 and 12 km. In fact, the analysis made by *Kondo et al.* [1999] showed that the CN fine particle concentration positively correlated with the NO_x mixing ratio and NO_x/NO_y ratio in the LS air masses obtained during SONEX. Moreover, the slope of the positive correlation between the CN and NO_x values was generally close to the median value of the ratio between the enhanced levels of NO_y (δNO_y) and CN (δCN) found in the aircraft plumes ($\delta NO_y/\delta CN$ = 0.11 pptv STP-cm^3). They concluded that an

increase in CN particles due to aircraft emissions constituted 29 % of the observed CN fine particle concentration. These results suggest that air masses with low CN values can be used as background in the LS. A positive correlation between the CN concentration and NO_x/NO_y ratio was also found in the UT in air masses with CN < 5000 STP-cm^{-3} (Figure 6). Although the overall correlation was partly due to the vertical profile of CN and NO_x/NO_y, a positive correlation was generally found even within each 1 km layer and within limited O_3 ranges. These results suggest that aircraft emissions played some role as a source of CN in the UT air masses sampled during SONEX. Using the SONEX data, *Anderson et al.* [1999] estimated that 8 % of the CN fine particles in the northern hemispheric UT originated from aircraft emissions, based on the emission index of CN obtained within the aircraft plumes. However, it should be noted that when a clear enhancement of NO and NO_y due to lightning activity was seen during the above-mentioned four flights, an enhancement of CN concentration up to 3_10^4 STP-cm^{-3} was also seen. New particle formation in the cloud-scavenged air around cumulous clouds can elevate the CN concentration in the UT [e.g., *Clarke et al.*, 1998]. Consequently, although low CN air masses were considered to be relatively unaffected by aircraft emissions, high CN air masses were not necessarily affected greatly. For the present analysis, air masses with a CN concentration lower than 1500 and 1000 STP-cm^{-3} were used to make a reference NO_y-O_3 relationship in the UT and LS, respectively, irrespective of the location in which they were sampled. A different criterion was chosen because the CN concentration was systematically higher in the UT than in the LS (Figure 5). These data corresponded to 28 and 47 % of the UT and LS data. As for the "low ΔNO_y reference", a median NO_y value was calculated for each 10 ppbv O_3 range and a linear relationship was calculated for the UT and LS data separately (Figure 4, denoted as the "low CN reference" hereafter). The dNO_y values were calculated for every 10-s data using this relationship.

3.2. Validity and Uncertainty in the dNO_y Estimate

3.2.1. Reference values. The median values of the dNO_y calculated using the two references are shown in Table 1 for both the UT and LS data. The median dNO_y values for each 1 km layer are

also shown for the tropospheric data in the NAFC region (Figure 7). In this case, the dNO_y values were calculated down to 6.5 km, although the reference was derived using the data at 8.5 – 11.5 km. The two sets of dNO_y values were generally in good agreement when relatively large uncertainties were considered. Because the two definitions of the background air mass had quite different characteristics, the agreement between the two sets of dNO_y values confirmed the validity of the method adopted in this study. The dNO_y values calculated using the low CN reference were slightly lower when compared to those calculated using the low ΔNO_y reference. The median of the differences in the dNO_y values was 8 and 18 pptv in the UT and LS, respectively, suggesting the uncertainty in the dNO_y estimation caused by selecting the background air mass. Since the difference in the two sets of the dNO_y values was small and systematic, the values calculated from the low ΔNO_y reference are used in the following discussion. Although it is not shown here, similar results were also obtained when the dNO_y value was calculated using the N_2O-NO_y relationship in the LS instead of using the NO_y-O_3 one.

3.2.2. Correlation. In Figure 8, a correlation plot between dNO_y and ΔNO_y is shown for the UT NAFC data (8.5 – 11.5 km). In this figure, the median dNO_y values for each 50 pptv range in the ΔNO_y values and a one-to-one line are also shown. A large variability was generally seen in the dNO_y values presumably reflecting the wide variety of air mass histories. However the median values of dNO_y generally increased with the ΔNO_y values suggesting that the averaged dNO_y values were reasonable estimates for the aircraft impact on reactive nitrogen. The dNO_y values were generally lower than the ΔNO_y values, partly due to the fact that when the ΔNO_y value was higher, the NO_y value in the real atmosphere tended to decrease more because of dilution.

On the other hand, the dNO_y value in the UT did not increase with either the CO or C_2H_2 value both in the NAFC and US continent regions (not shown), suggesting that the high dNO_y values were generally not due to the convective transport of polluted air masses.

3.2.3. Influence from lightning. One of the largest error sources, which can result in

overestimating the dNO_y values in the UT, is influence from NO production by lightning. As described above, the data, which had a clear signature of NO production by lightning (i.e., distinct enhancement in the NO and NO_y mixing ratios and the NO_x/NO_y ratio), was excluded from the present analysis. However, these were the only cases in which data were removed showing the influence of recent NO production by lightning. Lightning activity generally has an effect similar to aircraft emissions: it increases the NO_x and NO_y mixing ratios, the NO_x/NO_y ratio, and the CN concentration. In order to estimate the effect of aircraft on air masses which had been minimally affected by lightning, dNO_y values were calculated using only air masses which had remained over the Atlantic Ocean more than 90 % of time within 5-d prior to the measurements. This criterion was used because most lightning activities occur over land [e.g. *Turman and Edger* 1982]. In addition, air masses which had passed near the Florida Peninsula were also excluded because of the intensive lightning activity in that region. The selected data consisted of 27 % of the UT data in the NAFC region. As a result, the median dNO_y values in the 9.5-11.5 km range where the largest dNO_y values were obtained decreased by 24 %. Because these air masses generally came from lower latitudes where aircraft NO_x emissions were lighter, the reduction in dNO_y values could also have been the result of the change in the effect of aircraft. However, this change in the dNO_y value provides an estimate of the degree of possible overestimation of the effect of aircraft in this study.

3.2.4. Stagnated air mass within the NAFC region. A clear indication that aircraft emissions had caused an increase in dNO_y was seen in air masses sampled during the flight made at the eastern NAFC region on 971023 (Figure 1). The correlation plot of NO_x-dNO_y obtained during this flight is shown in Figure 9. Most of the dNO_y was found to be in the form of NO_x, suggesting that the NO_x input had been made within the lifetime of NO_x of about 5 days (UT at 40N-60°N). The 10-day back trajectories of the air masses obtained during this flight are shown in Figure 10. As shown in this figure, these air masses remained over the ocean in last 10-d and stagnated in the NAFC region the last 5-d. The median value of the O_3 and CO mixing ratios in the UT (8.5-11.5 km) were 37 and 77 ppbv and they changed little throughout the flight. Consequently, most of the change

in NO_x and NO_y was quite likely due to aircraft emissions. The median and maximum value of the ΔNO_y(10-d) were 71 and about 300 pptv, respectively, at altitudes between 9.5 and 11.5 km. Almost all of the input from aircraft was made within the last 5-d in this calculation. The median and maximum value of the dNO_y were 42 and about 200 pptv, respectively, in the 9.5-11.5 km altitude range. These data clearly indicate that aircraft emissions can raise the levels of NO_x and NO_y over a large region and the effect was successfully detected by the method used in this study.

3.3. Vertical Profile of dNO_y

In the NAFC region of the troposphere, the dNO_y values were close to zero at altitudes between 7 and 9 km, suggesting minor impact from aircraft emissions (Figure 7). At altitudes above 9 km, dNO_y increased with altitude, reaching 43 and 71 pptv at 10 and 11 km, respectively. (37 and 66 pptv at these two altitudes when the low CN reference was used.) The medians of the dNO_y/NO_y ratio at these two altitudes were 16 and 21 %; i.e., about 20 % of the NO_y in the UT likely originated from aircraft emissions. These results are also summarized in Table 1.

As described above, the model input NO_x value along the air mass trajectory, ΔNO_y, was calculated for each data point. Consequently, a statistical analysis can be made on the ΔNO_y value for the same data set from which the dNO_y values were calculated. In Figure 7, the median values of ΔNO_y for the 5-d and 10-d trajectories are shown. The median ΔNO_y(10-d) was 25 pptv at 9 km and increased with altitude reaching 160 pptv at 11 km. The shape of the profile is consistent with the that of the dNO_y value, although the dNO_y values were systematically lower than the ΔNO_y values, a likely result of the dilution effect.

The median value of dNO_y in the UT over the US continent region was calculated using all of the data obtained at 8.5-11.5 km range (Figure 11 and Table 1). This was because the amount of the data was not sufficient to derive a vertical profile of the dNO_y values. The median value was 32 pptv, comparable to the 28 pptv in the NAFC region. Although the data over the US continent was obtained from only two flights and the amount of data was smaller (4790 versus 1539 10-s data), the results here suggest a similar effect from aircraft emissions in the two regions.

The median value of dNO_y in the LS was calculated for the 8.5-11.5 km range (Figure 11 and Table 1). The median values of dNO_y and dNO_y/NO_y in the NAFC region were 128 pptv and 16 %, respectively. (110 pptv and 14 % when the low CN reference was used.) The median dNO_y value over the US continent region was 89 pptv, again comparable to the NAFC value when the large central 67 % ranges are considered. It should be noted that these dNO_y values were systematically higher than those in the UT both in the NAFC and US continent regions, 28 pptv versus 89 pptv in the NAFC region. The contrast in the dNO_y values between the UT and LS was much higher than that in the ΔNO_y(10-d) values, at least in the NAFC region (72 pptv versus 102 pptv). One possible explanation is the longer residence time of NO_y in the LS than in the UT. In the UT, the NO_y level can be lowered by dry and wet deposition of HNO_3 and aerosol nitrates through the vertical mixing of air. In the LS, NO_y cannot be lost until the air mass is transported into the troposphere. *Gettelman* [1998] estimated the residence time was around 50-d for aircraft exhaust released in the LS (lowermost stratosphere) using the NASA 1992 zonal mean aircraft emission database. During SONEX, all the stratospheric air masses were sampled in the LS as described above. Since the tropopause height was lower during late autumn, a larger amount of NO_x could have been injected into the LS and the LS air masses might have been influenced by the accumulated effect.

3.4. Relationship of dNO_y with NO_x/NO_y, CN, and O_3

In Figures 12a-12d, the correlation plots between the dNO_y and NO_x/NO_y values and between the dNO_y and CN values are shown for the UT and LS using the data from both the NAFC and the US continent regions. For these figures, we used only the data in which the model input NO_x values during the last 5-d were greater than 80 % of the 10-d values (i.e., $\Delta NO_y(5\text{-d})/\Delta NO_y(10\text{-d}) > 0.8$). This is because NO_x molecules emitted from aircraft more than 5-d prior to the measurements could have already been converted to higher oxidized species, such as HNO_3. In fact, this data selection generally improved the degree of correlation. The lifetime of NO_x was estimated to be 4.8 and 3.2-d in the UT and LS (O_3=100-200 ppbv), respectively, at 40°N – 60°N using the observed values of aerosol surface area etc. In Figure 12a, the dNO_y values were plotted against the NO_x/NO_y ratios

obtained in the UT. Different symbols were used for the data where O_3 = 0-50 ppbv and 50-100 ppbv, respectively. The NO_x/NO_y ratio generally increased with dNO_y in both data sets. This is consistent with the fact that emissions of NO_x from aircraft increases both the NO_x/NO_y ratio and dNO_y value. In other words, the change in the NO_x/NO_y ratio observed in the UT during SONEX was partly due to NO_x from aircraft emissions. A positive correlation observed in the air masses where O_3 = 0 – 50 ppbv was mostly due to those sampled on 971023 which had been strongly affected by aircraft emissions as described above. The degree of the NO_x/NO_y increase was higher for air masses where O_3 = 0-50 ppbv than that for air masses where O_3 = 50-100 ppbv when data with same dNO_y value was compared. This result is plausible because the NO_y value was generally lower when O_3 was low (Plate 1) and the NO_x input could cause a greater change in the NO_x/NO_y ratio.

In Figure 12b, dNO_y values were plotted against the CN concentration obtained in the UT. *Kondo et al.* [1999] and *Anderson et al.* [1999] calculated the ratio between enhanced levels of NO_y (δNO_y) and CN (δCN) observed within aircraft plumes. The $\delta NO_y/\delta CN$ ratio ranged between 0.04 and 0.2 pptv STP-cm^3 with a median value of 0.11 pptv STP-cm^3. In Figure 12b, two lines having this slope and different intercepts are also plotted. As seen in this figure, the dNO_y value had a weak positive correlation with the CN concentration in both the air masses where O_3 = 0-50 ppbv and 50-100 ppbv. Based on the PCASP measurements, the median value of the aerosol surface area for aerosol particles with diameters between 0.1 and 3.0 μm was 1.7 μm^2 cm^{-3} in the UT in the NAFC region. Under this condition, CN is lost primarily by the Brownian coagulation with CN, for CN concentrations higher than about 1400 STP-cm^{-3}. The half-lifetime of CN with a diameter of 15 nm at a CN concentration of 2500 STP-cm^{-3} is 1.3 days and decreases inversely with the CN mixing ratio [*Pruppacher and Klett*, 1997; *B.Liley*, personal communication 1999]. Because the lifetime of CN was shorter than that of NO_x and NO_y, the CN concentration should be generally lower than that expected from the slope in the aircraft plumes if aircraft emissions were the dominant source of CN. Consequently, the observed result was not inconsistent with the hypothesis that aircraft emissions contributed to a source of CN for air masses where O_3 = 50-100 ppbv. On the other hand, other CN

sources were predominant for air masses where O_3 = 0 – 50 ppbv, because much higher CN concentrations than those expected from aircraft emissions were observed in these air masses. In fact, no correlation between CN and NO_x/NO_y was found for air masses where CN > 5000 STP-cm^{-3} as described above (Figure 6). However it should be noted that a positive correlation having a similar slope to that within the aircraft plumes was seen in a part of air masses. As described above, air masses sampled on 971023 had probably been strongly affected by aircraft emissions (see Sub-section 3.2.4.) and the O_3 values in these air masses were mostly below 50 ppbv. The data where NO_x was higher than 60 pptv obtained on this day were shown using a different symbol in Figure 12b and their CN-dNO_y slope was found to be generally similar to that observed within the aircraft plumes. Consequently, aircraft emissions could have caused an increase in the CN concentration in the UT in some cases during SONEX, resulting in the positive correlation between CN and dNO_y, and CN and NO_x/NO_y, although the background level of the CN concentration was changed greatly by other CN sources.

In Figure 12c, the correlation plot between dNO_y and the NO_x/NO_y ratio in the LS is shown. A positive correlation was generally found in the LS. Because the LS air mass was generally free from tropospheric reactive nitrogen sources, the results shown here strongly suggest that an NO_x input from aircraft emissions primarily caused the NO_x variation in the LS.

In Figure 12d, the correlation plot between dNO_y and CN in the LS is shown. A clear positive correlation between the two parameters was found suggesting that aircraft emissions were an important source of CN in the LS. The slope between dNO_y and CN was generally smaller as compared to the median $\delta NOy/\delta CN$ ratio of 0.11 pptv STP-cm^3 observed in aircraft plumes. This is reasonable because the lifetime of NO_y is much longer than that of CN in the LS.

In Figures 13a and 13b, the correlation plots between dNO_y and O_3, and NO_x/NO_y and O_3 are shown using both the UT and LS data in the NAFC region. The median values of dNO_y or NO_x/NOy in seven O_3 ranges are also shown. Systematically large dNO_y values were generally found with O_3 values between 75 and 125 ppbv. The dNO_y values were generally distributed around zero for lower and higher O_3 air masses. These features are quite similar to those of the correlation plot between

NO_x/NO_y and O_3, suggesting a relatively greater effect from aircraft emissions in the air masses with O_3 values between 75 and 125 ppbv. These air masses are considered to have remained generally around the tropopause altitude where NO_x input from aircraft emissions is large. Air masses with a lower O_3 mixing ratio in the UT could generally be more strongly influenced by lower altitude air. This is consistent with the fact that the dNO_y values were close to zero when the CO and C_2H_2 values were high. Similarly, air masses with O_3 values higher than 125 ppbv are considered to be less affected by aircraft emissions. Further decreases in the NO_x/NO_y ratio with an increasing O_3 value between 125 and 300 ppbv were likely because the loss rate of NO_x via heterogeneous hydrolysis of N_2O_5 is higher for higher O_3 values. Similar O_3 dependence of the dNO_y and NO_x/NO_y values was also seen in the air masses obtained over the US continent in the UT and LS. In this case, high NO_x/NO_y ratios up to 0.3 were observed with O_3 values as high as 160 ppbv.

3.5. Estimation of dNOx in the UT

The ratio between excess NO_x (dNO_x) and dNO_y was estimated from the following expression:

$$\frac{dNOx}{dNOy} = \frac{NOx}{NOy} - \frac{NOx}{NOy}_{ref} (1-\gamma) \frac{1}{\gamma} \quad (1)$$

where $\gamma = dNO_y/NO_y$. To make the reference NO_x/NO_y ratio, we used the background air masses what were used to make the reference NO_y-O_3 relationship, i.e., air masses with ΔNO_y(10-d) values (model NO_x input along the 10-d back trajectory) lower than 40 pptv. In Figure 14, a vertical profile of the median NO_x/NO_y ratio in the background air masses is shown with that in air masses in the NAFC region. The NO_x/NO_y ratios in the NAFC region were systematically higher than those in the background air masses. Using these NO_x/NO_y values and the dNO_y/NO_y values shown in Table 1 (low ΔNO_y(10-d) reference), dNO_x/dNO_y was calculated for each 1 km altitude level. As a result, the dNO_x/dNO_y ratio was estimated to be 0.54 and 0.38 at altitudes of 10 and 11 km, respectively. Even if the median NO_x/NO_y values in the low CN air masses were used for the reference, similar results

were obtained (Figure 14). Furthermore, even if only the data at 45°N – 60°N were used for the reference to eliminate a possible effect from the change in the NO_x/NO_y ratio with latitude, similar results were obtained. These results suggest that about half of the excess NO_y was likely to be in the form of NO_x in the UT. Using an average dNO_x/dNO_y value of 0.46, we found the excess NO_x to be 20 and 33 pptv at 10 and 11 km, respectively.

The dNO_x/NO_x ratio can be also expressed using the NO_x/NO_y ratio and dNO_y/NO_y ratio by transforming the equation (1). Using the same values shown above, we estimated that 30 % of the NO_x at 10 and 11 km was likely to have originated from aircraft emissions in the UT.

4. Summary

The large scale impact of aircraft emissions on reactive nitrogen in the UT and LS was estimated using the NO_y-O_3 correlation obtained during SONEX, which was carried out over the US continent and NAFC region in October and November 1997. For the present analysis, we excluded data obtained within aircraft plumes, data clearly influenced by NO production by lightning, and data influenced by recent convective transport of air affected by surface sources. Two reference NO_y-O_3 relationships in the air masses, which were considered to be affected little by aircraft emissions, were made using the data obtained above 8.5 km. First, the integrated input of NO_x into an air mass along a 10-d back trajectory (ΔNO_y) was calculated based on the ANCAT/EC2 aircraft emission inventory. When the ΔNO_y value was less than 40 pptv (lower 42 and 37 % values in the UT and LS), that air mass was used to make a reference NO_y-O_3 relationship, irrespective of the location from which it was sampled. Second, air masses with a CN concentration lower than 1500 and 1000 STP-cm^{-3} (lower 28 and 47 % values) in the UT and LS were used to make the reference. Using these two reference NO_y-O_3 relationships, the two sets of the excess NO_y (dNO_y) were calculated from observed values of NO_y and O_3.

The two sets of dNO_y values generally agreed within 8 and 18 pptv in the UT and LS, respectively, in spite of the very different nature of the criteria for the background air selection. The calculated dNO_y values did not positively correlate with either the CO values or anthropogenically produced hydrocarbons such as C_2H_2, suggesting a negligible effect of the surface sources on the dNO_y values. On the other hand, the weak positive correlation between the dNO_y and ΔNO_y values indicated that the dNO_y values generally reflected the effect of aircraft emissions. By calculating the dNO_y values only for the air masses which remained over the ocean for 5-d prior to the measurement, the uncertainty in the dNO_y values due to the influence of recent NO production by lightning was estimated to be 24 %.

In the NAFC region (45°N – 60°N), the median value of dNO_y in the troposphere was close to zero between 7 and 9 km and increased with altitude above 9 km reaching 70 pptv (20 % of NO_y) at

11 km. High values of dNO_y and NO_x/NO_y ratio were generally found in air masses in which O_3 = 75 – 125 ppbv, suggesting a stronger effect around the tropopause. The median value of dNO_y in the LS in the NAFC region at 8.5 – 11.5 km was about 120 pptv. The larger dNO_y value observed in the LS was probably the result of the accumulated effect of aircraft emissions, given the long residence time of the affected air in the LS (50 days).

In general, the dNO_y value positively correlated with the NO_x/NO_y ratio in both the UT and LS in the NAFC and the US continent regions, suggesting that the observed large scale changes in the NO_x/NO_y levels and NO_x values in the UT and LS were partly caused by NO_x from aircraft emissions. The slope of the positive correlation between the dNO_y and CN values in the LS was generally consistent with that observed in the aircraft plumes, suggesting the importance of aircraft emissions as a source of CN in the LS. A positive correlation between the dNO_y and CN values was also seen in a part of air masses in the UT and its slope was not inconsistent with that observed in the aircraft plumes; however, the significance of aircraft emissions is still not clear.

The ratio between excess NO_x (dNO_x) and dNO_y was calculated using the reference NO_x/NO_y ratio. In the UT (NAFC region), it was estimated that about half of dNO_y was in the form of NO_x (20 and 33 pptv at 10 and 11 km) and about 30 % of the NO_x had originated from aircraft emissions. These estimates were generally consistent with the results from the model calculations.

In this study, the degree of the large scale impact of aircraft emissions on reactive nitrogen was estimated from the observed data. A more quantitative estimate will be made using sophisticated three-dimensional models when they can consistently reproduce most of the observed features of various species.

Acknowledgments. We are indebted to all of the SONEX participants for their cooperation and support. Special thanks are due to the flight and ground crews of the NASA DC-8 for helping make this effort a success. We thank M. Kanada and H. Jindo for their technical assistance with the measurements of NO and NO_y. We also thank B. Liley at NIWA, New Zealand, and L. Jaegle at Harvard University, for calculating the lifetime of CN and NO_x, respectively. This work was supported in part by the Ministry of Education, Science, Sports, and Culture.

References

Anderson, B.E., et al., An assessment of aircraft as a source of particles to the upper troposphere, *Geophys. Res. Lett.* in press, 1999.

Baughcum, S.L., T.Z. Tritz, S.C. Henderson, and D.C. Pickett, Scheduled civil aircraft emissions inventories for 1992: Database development and analysis, *NASA Contr. Rep.4700*, 1996.

Brasseur, G.P., J.-F. Muller, and C. Granier, Atmospheric impact of NO_x emissions by subsonic aircraft: A three-dimensional model study, *J. Geophys. Res.*, *101*, 1423-1428, 1996.

Brasseur G.P., R.A. Cox, D. Hauglustaine, I. Isakusen, J. Lelieveld, D.H. Lister, R. Sausen, U. Schumann, A. Wahner, and P. Wiesen, European scientific assessment of the atmospheric effects of aircraft emissions, *Atmos. Environ.*, *32*, 2329-2418, 1998.

Clarke, A.D., J.L. Varner, F. Eisele, R.L. Mauldin, D. Tanner, and M. Litchy, Particle production in the remote marine atmosphere: Cloud outflow and subsidence during ACE 1, *J. Geophys. Res.*, *103*, 16,397-16,409, 1998.

Gardner, R.M. (Ed), ANCAT/EC2 aircraft emission inventories 1991/1992 and 2015: Final report, Produced by the ECAC/ANCAT and EC working group, 1998.

Gerz, T., T. Durbeck, and P. Konopka, Transport and effective diffusion of aircraft emissions, *J. Geophys. Res.*, *103*, 25,905-25,913, 1998.

Gettelman, A., The evolution of aircraft emissions in the stratosphere, *Geophys. Res. Lett.*, *25*, 2129-2132, 1998.

Hamm, S., G. Helas, and P. Warneck, Acetonitrile in the air over Europe, *Geophys. Res. Lett.*, *16*, 483-486, 1989.

Holton, J.R., P.H. Haynes, A.R. Douglass, R.B. Rood, and L. Pfister, Stratosphere – troposphere exchange, *Reviews of Geophysics*, *33*, 403-439, 1995.

Jaegle, L., D.J. Jacob, Y. Wang, W.H. Brune, D. Tan, I.C. Faloona, A.J. Weinheimer, B.A. Ridley, T.L. Campos, and G.W. Sachse, Sources of HOx and production of ozone in the upper troposphere over the United States, *Geophys. Res. Lett., 25*, 1709-17012, 1998.

Klemm, O., W.R. Stockwell, H. Schlager, and H. Zieries, Measurements of nitrogen oxides from aircraft in the northeast Atlantic flight corridor, *J. Geophys. Res.*, *103*, 31,217-31,229, 1998.

Koike, M., Y. Kondo, S. Kawakami, H. Nakajima, G.L. Gregory, G.W. Sachse, H.B.Singh, E.V. Browell, J.T. Merrill, and R.E. Newell, Reactive nitrogen and its correlation with O_3 and CO over the Pacific in winter and early spring, *J. Geophys. Res.*, *102*, 28,385-28,404, 1997.

Kondo, Y., H. Ziereis, M. Koike, S. Kawakami, G.L. Gregory, G.W. Sachse, H.B. Singh, D.D. Davis, and J.T. Merrill, Reactive nitrogen over the Pacific Ocean during PEM-West A, *J. Geophys. Res.101*, 1809-1828, 1996.

Kondo, Y., S. Kawakami, M. Koike, D.W. Fahey, H. Nakajima, N. Toriyama, M. Kanada, Y. Zhao,

G.W. Sachse, G.L. Gregory, The performance of an aircraft instrument for the measurement of NOy, *J. Geophys. Res.*, *102*, 28,663-28,671, 1997.

Kondo, Y., et al., Impact of aircraft emissions on NO_x in the lowermost stratosphere at northern midlatitudes, *Geophys. Res. Lett.* in press, 1999.

Lamarque et al., Three-dimensional study of the relative contributions of the different nitrogen sources in the troposphere, *J. Geophys. Res*, *101*, 22,955-22,968, 1996.

Mahieu. E., C.P. Rinsland, R. Zander, P. Demoulin, L. Delbouille, and G. Roland, Vertical column abundances of HCN deduced from ground-based infrared solar spectra: Long-term trend and variability, *J. Atmos. Chem.*, *20*, 299-310, 1995.

Murphy, D.M., D.W. Fahey, M.H. Proffitt, S.C. Liu, K.R. Chan, C.S. Eubank, S.R. Kawa, and K.K. Kelly, Reactive nitrogen and its correlation with ozone in the lower stratosphere and upper troposphere, *J. Geophys. Res.*, *98*, 8751--8773, 1993.

Pickering, K.E., A.M. Thompson, L. Pfister, T.L. Kucsera, Y. Kondo, G.W. Sachse, B.E. Anderson, and D.R. Blake, Comparison and interpretation of chemical measurements from two SONEX flights over the Canadian maritimes: Lightning, convection, and aircraft signatures, *this issue.*

Pruppacher, H.R., and J.D. Klett, Microphysics of clouds and precipitation, Kluwer Academic Publications, 1997.

Ridley, B.A., J.G. Walega, J.E. Dye, and F.E. Grahek, Distribution of NO, NO_x, NO_y, and O_3 to 12 km altitude during the summer monsoon season over New Mexico, *J. Geophys. Res.*, *99*, 25519--25534, 1994.

Rinsland, C.P, M.A.H. Smith, P.L. Rinsland, A. Goldman, J.W. Brault, and G.M. Stokes, Ground-based infrared spectroscopic measurements of atmospheric hydrogen cyanide, *J. Geophys. Res.*, *87*, 11,119-11,125, 1982.

Schlager, H., P. Konopka, P. Schulte, U. Schumann, H. Ziereis, F. Arnold, M. Klemm, D.E. Hagen, P.D. Whitefield, and J. Ovarlez, In situ observations of air traffic emission signatures in the North Atlantic flight corridor, *J. Geophys. Res.*, *102*, 10,739-10,750, 1997.

Shetter, R. E., and M. Müller, Photolysis frequency measurements using actinic flux spectroradiometry during the PEM-Tropics mission: Instrumentation description and some results, *J. Geophys. Res.*, *104*, 5647-5661, 1999.

Simpson, I., D. R. Blake, N. J. Blake, T-Y. Chen, J. P. Lopez, B. C. Sive, F. S. Rowland, Nonmethane hydrocarbon measurements in the North Atlantic flight corridor during SONEX, *this issue.*

Singh, H.B., A.M. Thompson, and H. Schlager, 1997 SONEX/POLINAT-2 airborne missions: Overview and accomplishments, *Geophys. Res. Lett.* in press, 1999.

Sugita, T., Y. Kondo, M. Koike, K. Kita, Y. Zhao, S. L. Baughcum, S. A. Vay, B. E. Anderson, G. W. Sachse, N. Toriyama, and S. Matsukawa· NO_x emission indices observed during the

SONEX mission, *in preparation*, 1999.

Thompson, A.M., et al., The Goddard/Ames meteorological support and modeling system during SONEX: Evaluation of analyses and trajectory-based model products with tracer data, *this issue.*

Turman, B. N. and B. C. Edgar, Global lightning distribution at dawn and dusk, *J. Geophys. Res.*, *87*, 1191-1206, 1982.

Witte, J.C., I.A. Folkins, J. Neima, B.A. Ridley, J.G. Walega, and A.J. Weinheimer, Large-scale enhancements in NO/NOy from subsonic aircraft emissions: Comparison with observations, *J. Geophys. Res.*, *102*, 28,169-28,175, 1997.

Ziereis, H, and F. Arnold, Gaseous ammonia and ammonium ions in the free troposphere, *Nature*, 321, 503-505, 1986.

Figure 8. Correlation plot between dNO_y and ΔNO_y(10-d) for air masses obtained in the UT (8.5-11.5 km) in the NAFC region. The median values and central 67 % ranges are also shown in six O_3 ranges. A one-to-one line is also shown.

Figure 9. Correlation plot between NO_x and dNO_y for the flight made on 971023 at 8.5-11.5 km.

Figure 10. Ten-day back trajectory of air mass sampled in every 30 minutes between 0830 and 1100 UT during the flight made on 971023. Diamonds on the trajectories denote the location of air masses 5-d prior to the measurement.

Figure 11. Median values and central 67 % ranges of the values of dNO_y (closed circles) in the 8.5-11.5 km layer. The median values of ΔNO_y(10-d) (crosses) are also shown.

Figure 12. Correlation plot for NO_x/NO_y – dNO_y and CN – dNO_y in the UT and LS at altitudes of 8.5-11.5 km. The air masses obtained in both the NAFC and the US continent regions were used. Only the air masses where ΔNO_y(5-d)/ΔNO_y(10-d) > 0.8 were used. A slope of the median value of the ratio between the increase in NO_y and CN observed in aircraft plumes ($\delta NO_y/\delta CN$ = 0.11 pptv STP-cm^3) is also shown in Figures 12b and 12d. The data obtained on 971023 in air masses where NO_x > 60 pptv are shown using a different symbol in Figure 12b. The O_3 values are in units of ppbv.

Figure 13. Correlation plot between (a) dNO_y – O_3 and (b) NO_x/NO_y – O_3 for the data obtained in the NAFC region. The median values and central 67 % ranges of the dNO_y and NO_x/NO_y ratio are also shown for the seven O_3 ranges.

Figure 14. Vertical profile of the NO_x/NO_y ratios in the troposphere in the NAFC region (closed circles). The values in the background air masses (open circles: low ΔNO_y(10-d) reference and crosses: low CN reference) are also shown. The median values and central 67 % ranges are shown for each 1 km.

Table 1. Median value of dNO_y

	--------- Ref 1 ---------				--------- Ref 2 ---------			
	pptv		%		pptv		%	
NAFC region								
Troposphere								
8.5 – 9.5 km	8	(-37~47)	3	(-15~17)	2	(-46~41)	1	(-19~15)
9.5 – 10.5 km	43	(-11~110)	16	(-4~34)	37	(-21~103)	13	(-7~32)
10.5 – 11.5 km	71	(-19~167)	21	(-6~35)	66	(-29~152)	18	(-10~34)
8.5 – 11.5 km	28	(-26~122)	11	(-10~29)	22	(-36~108)	8	(-13~28)
Stratosphere								
8.5 – 11.5 km	128	(-25~217)	16	(-3~27)	110	(-41~199)	14	(-5~25)
US region								
Troposphere								
8.5 – 11.5 km	32	(-64~108)	11	(-35~39)	25	(-70~102)	9	(-39~40)
Stratosphere								
8.5 – 11.5 km	89	(3~294)	13	(0~31)	71	(-13~277)	10	(-2~29)

Ref 1: Estimates using the low ΔNO_y (model input NO_x value along 10-d back trajectory) reference.
Ref 2: Estimates using the low CN reference.
The central 67 % ranges are shown in parentheses.

Authors' addresses

B.E. Anderson, G.L. Gregory, G.W. Sachse,
NASA Langley Research Center, Hampton, VA 23681-0001.
(b.e.anderson@larc.nasa.gov, g.l.gregory@larc.nasa.gov, g.w.sachse@larc.nasa.gov)

D. Blake,
Department of Chemistry, University California, Irvine, CA 92697.
(dblake@orion.oac.uci.edu)

H. Ikeda, M. Koike, Y. Kondo, and N.Toriyama, Y. Zhao,
Solar-Terrestrial Environment Laboratory, Nagoya University, Honohara, Toyokawa, Aichi, 442-8507, Japan.
(hibiki@stelab.nagoya-u.ac.jp, koike@stelab.nagoya-u.ac.jp, kondo@stelab.nagoya-u.ac.jp, toriyama@stelab.nagoya-u.ac.jp, yzhao@stelab.nagoya-u.ac.jp)

K. Kita,
Department of Earth and Planetary Physics, Faculty of Science, University of Tokyo, Hongo, Bunkyo-ku, Tokyo, Japan.
(kita@grl.s.u-tokyo.ac.jp)

S.C. Liu,
School of Earth and Atmospheric Sciences, Georgia Institute of Technology, 212 Bobby Dodd Way, Atlanta, GA 30332-0340.
(shaw.liu@eas.gatech.edu)

R. E. Shetter,
National Center for Atmospheric Research, 1850 Table Mesa Drive, Boulder, CO 80303.
(shetter@ncar.ucar.edu)

H.B. Singh,
NASA Ames Research Center, Moffett Field, CA 94035-1000.
(hsingh@mail.arc.nasa.gov)

T. Sugita,
National Institute for Environmental Studies, Onogawa, Tsukuba, Ibaraki, 305-0053, Japan.
(sugita@nies.go.jp)

A. Thompson,
NASA Goddard Space Flight Center, Greenbelt Road, Greenbelt, MD 20771-0001.
(thompson@gator1.gsfc.nasa.gov)

Plate 1

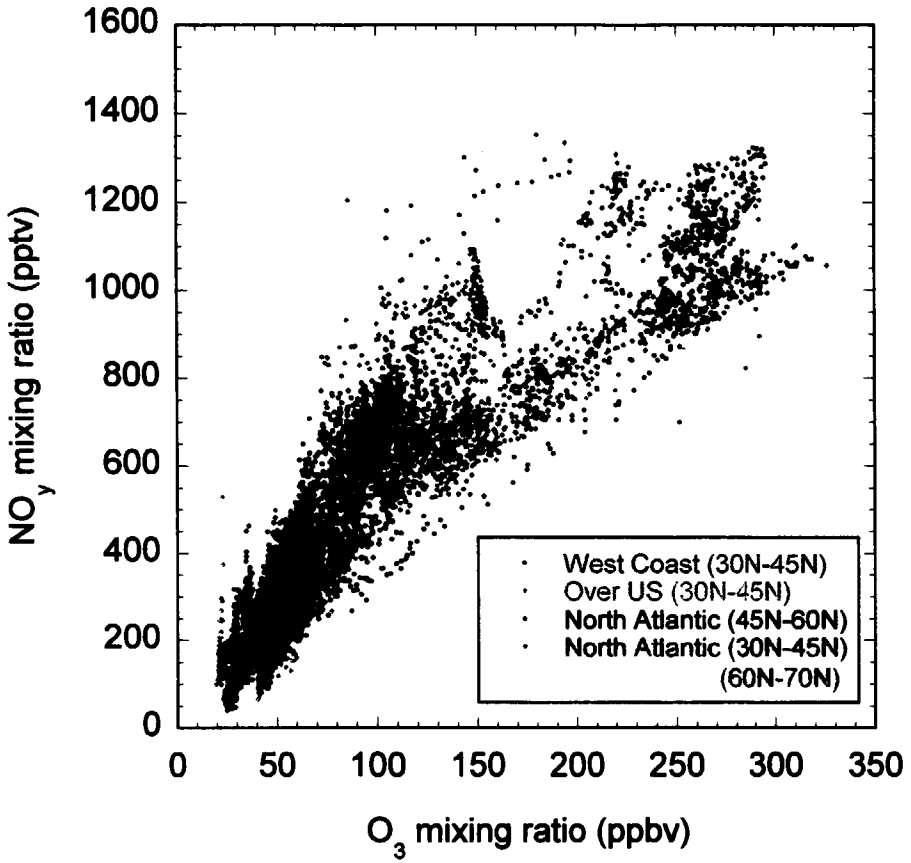
1600
1400
1200
1000
800
600
400
200
0
0
50
100
150
200
250
300
350
NO$_y$ mixing ratio (pptv)
O$_3$ mixing ratio (ppbv)
West Coast (30N-45N)
Over US (30N-45N)
North Atlantic (45N-60N)
North Atlantic (30N-45N)
(60N-70N)

Fig. 1

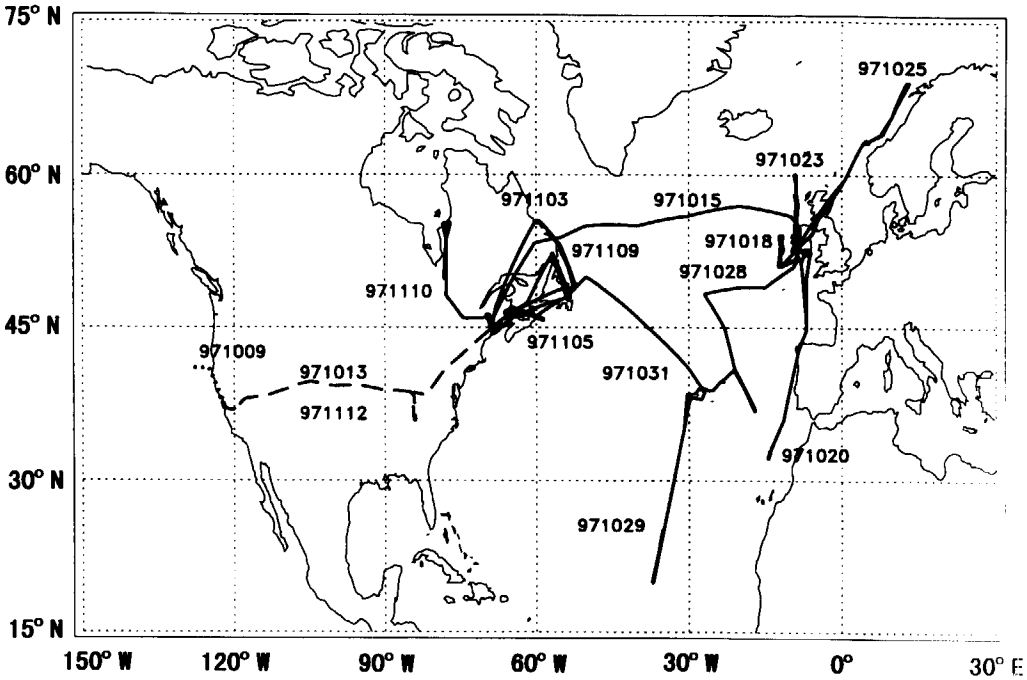
75° N
60° N
45° N
30° N
15° N
150° W
120° W
90° W
60° W
30° W
0°
30° E
971025
971023
971103
971015
971109
971018
971028
971110
971105
971009
971013
971031
971112
971020
971029

Fig. 2

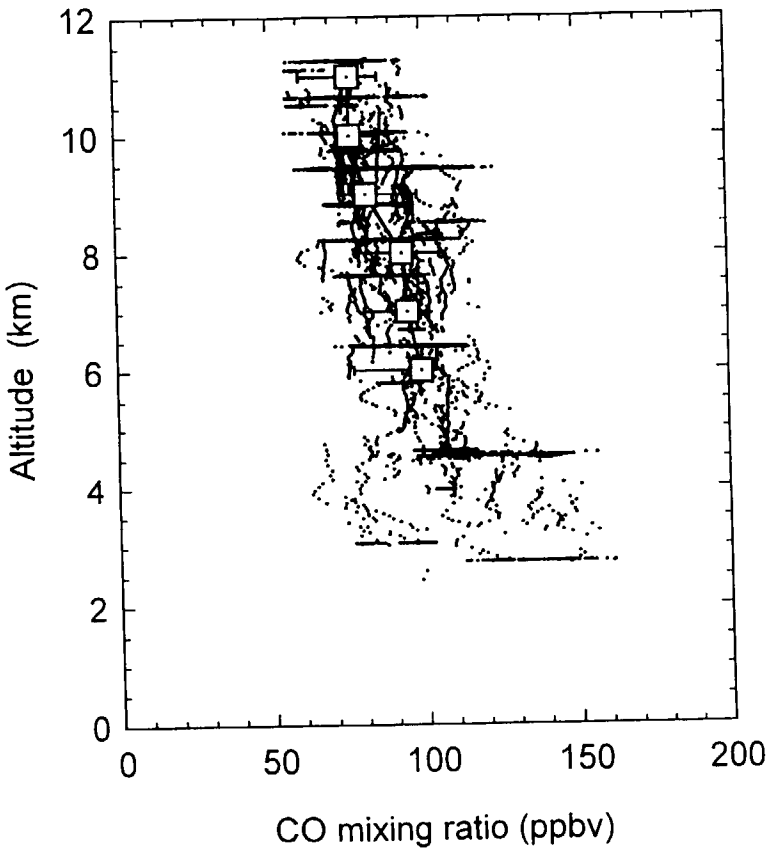
Altitude (km)
CO mixing ratio (ppbv)
0
2
4
6
8
10
12
0
50
100
150
200

Fig. 3

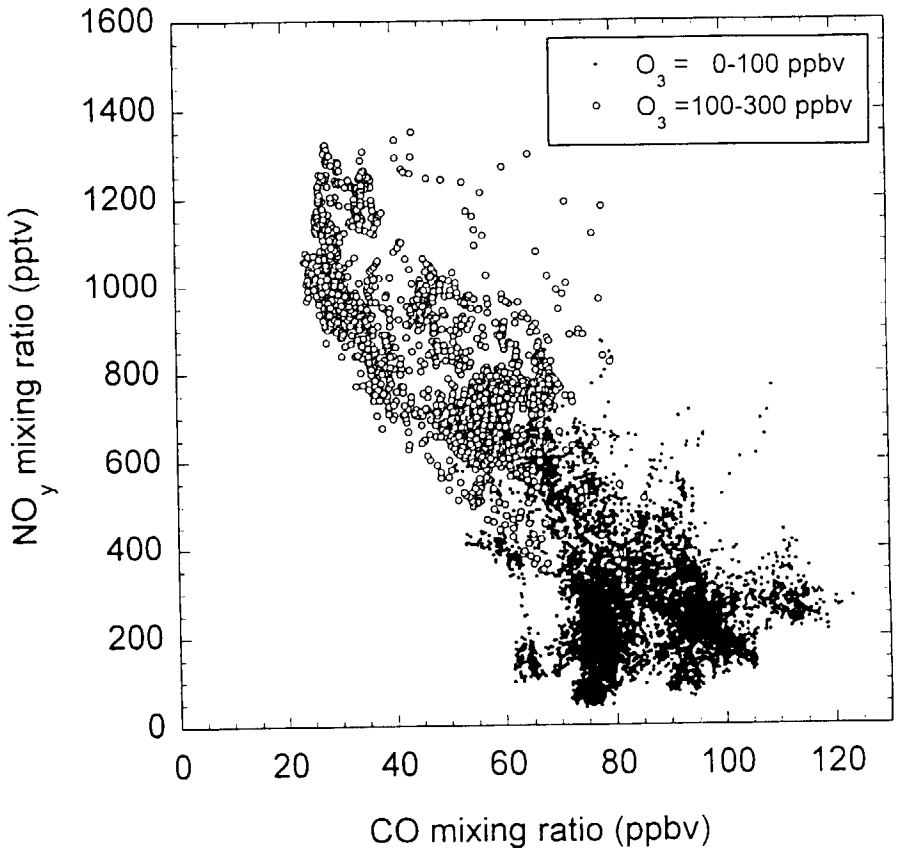
NO_y mixing ratio (pptv)
CO mixing ratio (ppbv)
O_3 = 0-100 ppbv
O_3 =100-300 ppbv
0
200
400
600
800
1000
1200
1400
1600
0
20
40
60
80
100
120

Fig. 4

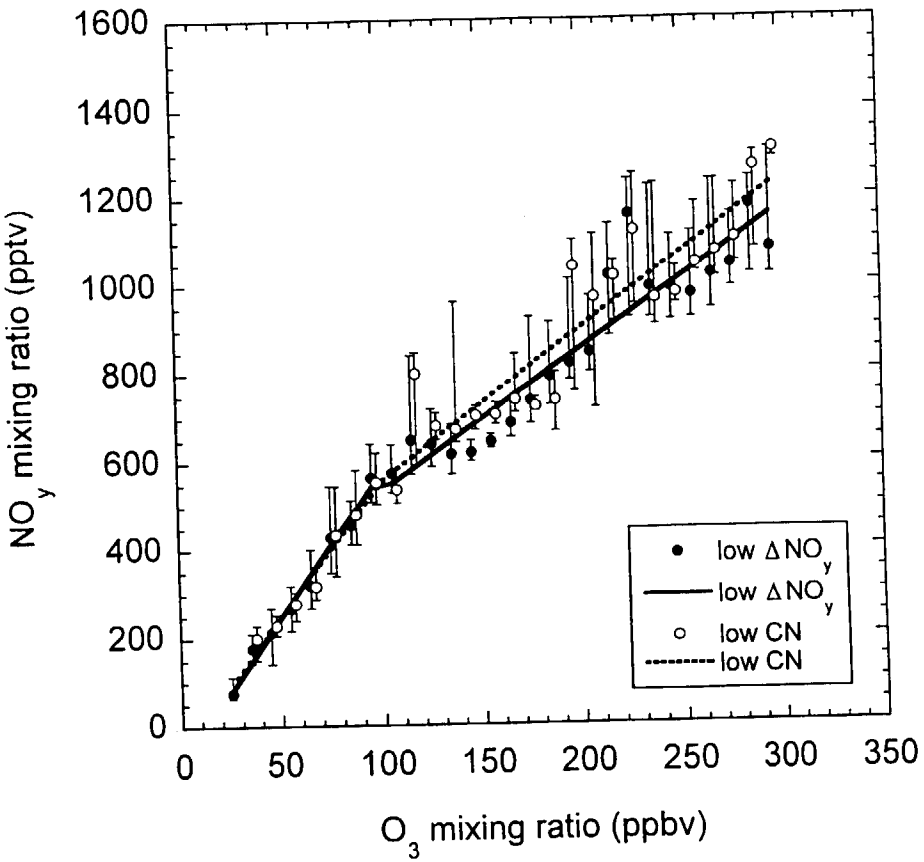
1600
1400
1200
1000
800
600
400
200
0
0
50
100
150
200
250
300
350
NO$_y$ mixing ratio (pptv)
O$_3$ mixing ratio (ppbv)
low ΔNO$_y$
low ΔNO$_y$
low CN
low CN

Fig. 5

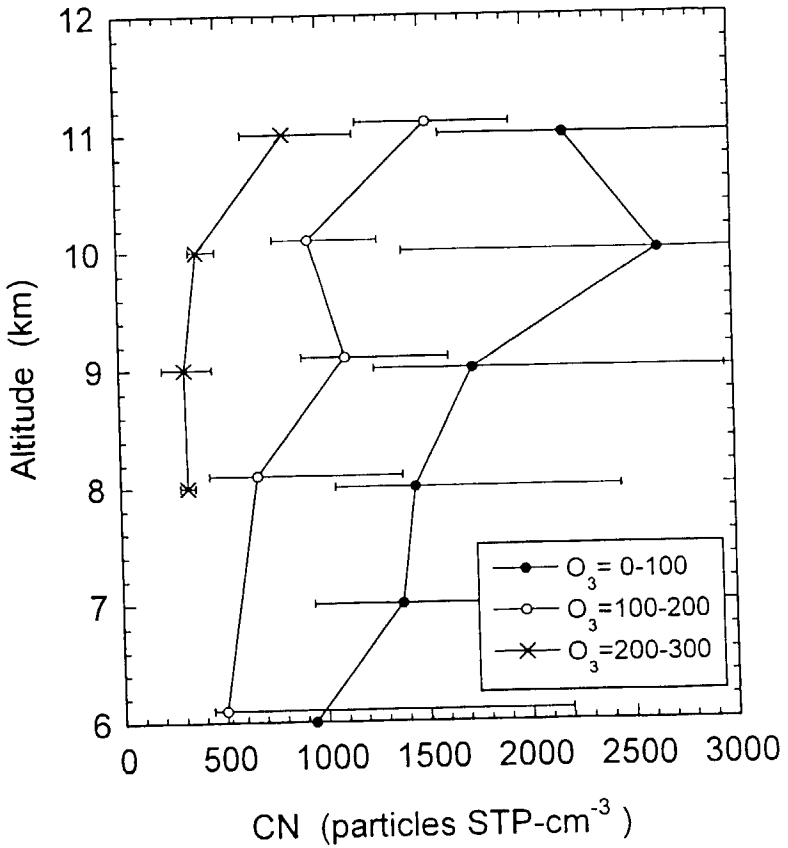
12
11
10
9
8
7
6
0
500
1000
1500
2000
2500
3000
Altitude (km)
CN (particles STP-cm^{-3})
O$_3$= 0-100
O$_3$=100-200
O$_3$=200-300

Fig. 6

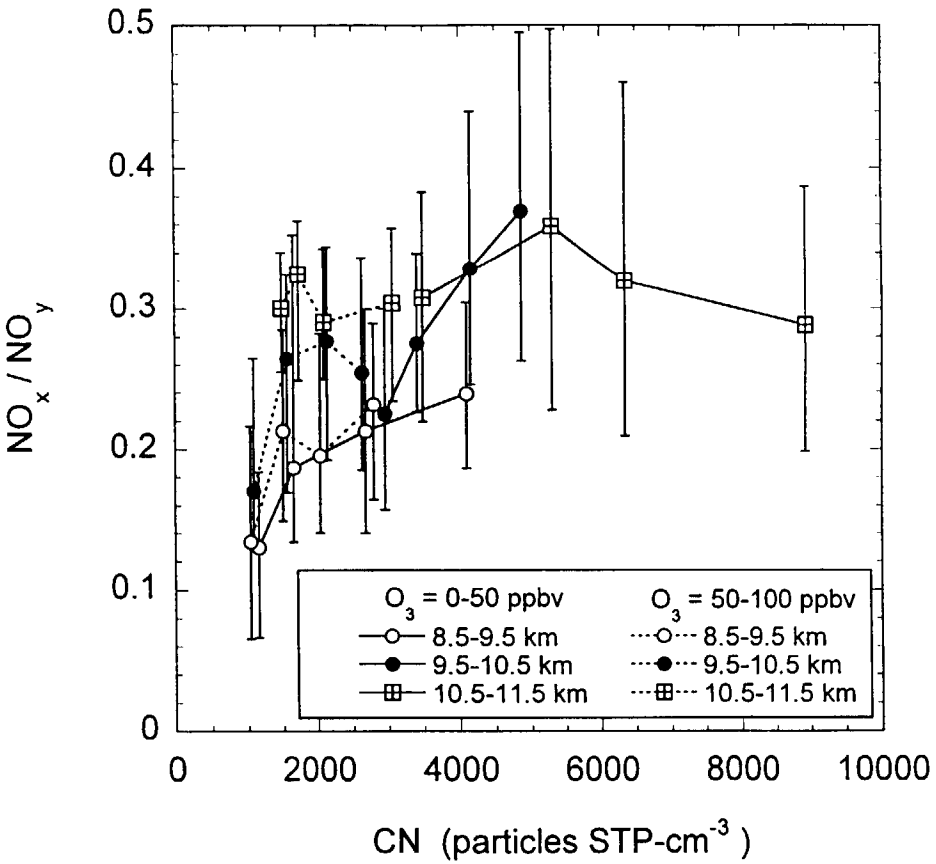
0.5
0.4
0.3
0.2
0.1
0
0
2000
4000
6000
8000
10000
NO_x / NO_y
CN (particles STP-cm^-3)
O3 = 0-50 ppbv
8.5-9.5 km
9.5-10.5 km
10.5-11.5 km
O3 = 50-100 ppbv
8.5-9.5 km
9.5-10.5 km
10.5-11.5 km

Fig. 7

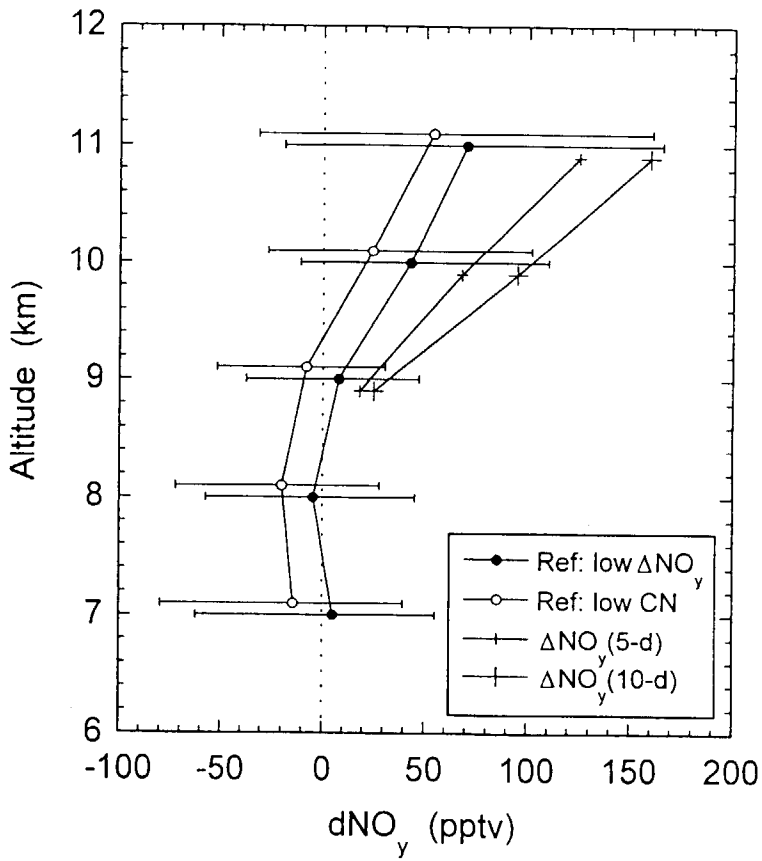
12
11
10
9
8
7
6
-100
-50
0
50
100
150
200
Altitude (km)
dNO_y (pptv)
Ref: low ΔNO_y
Ref: low CN
ΔNO_y (5-d)
ΔNO_y (10-d)

Fig. 8

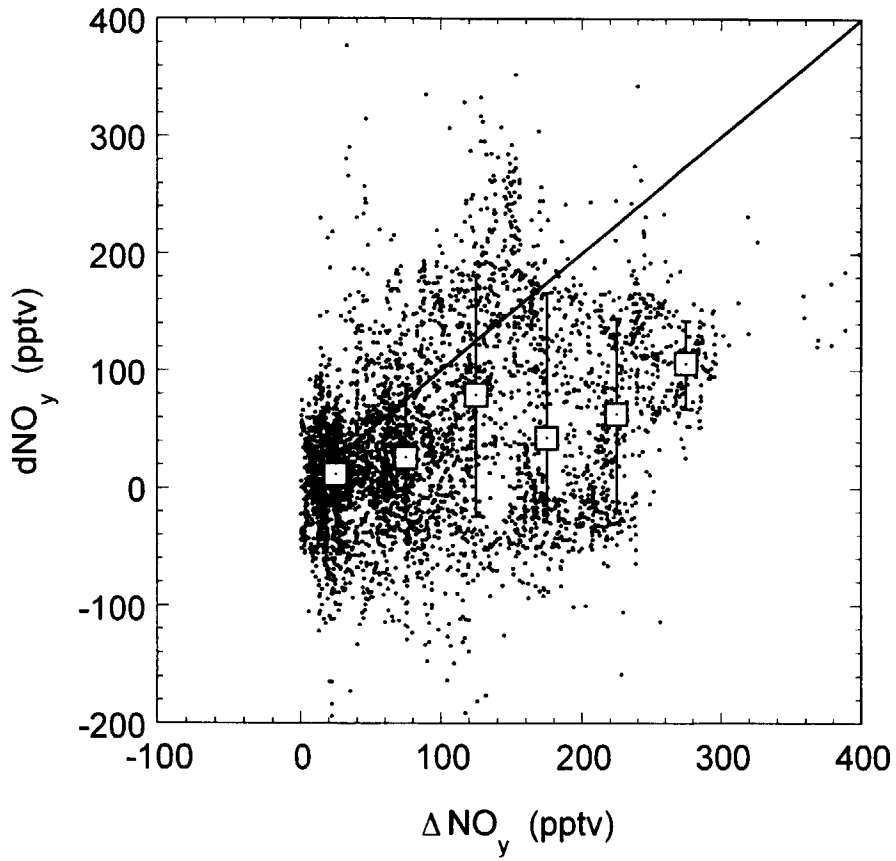
400
300
200
100
0
-100
-200
-100
0
100
200
300
400
dNO$_y$ (pptv)
Δ NO$_y$ (pptv)

Fig. 9

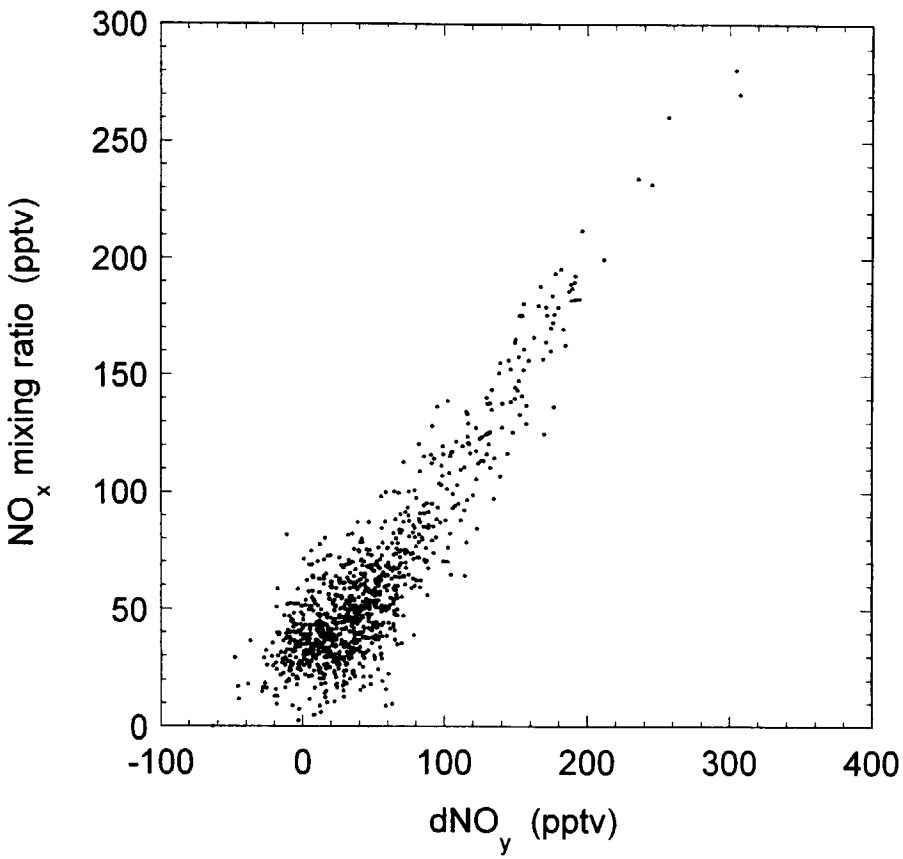
300
250
200
150
100
50
0
-100
0
100
200
300
400
NO$_x$ mixing ratio (pptv)
dNO$_y$ (pptv)

Fig. 10

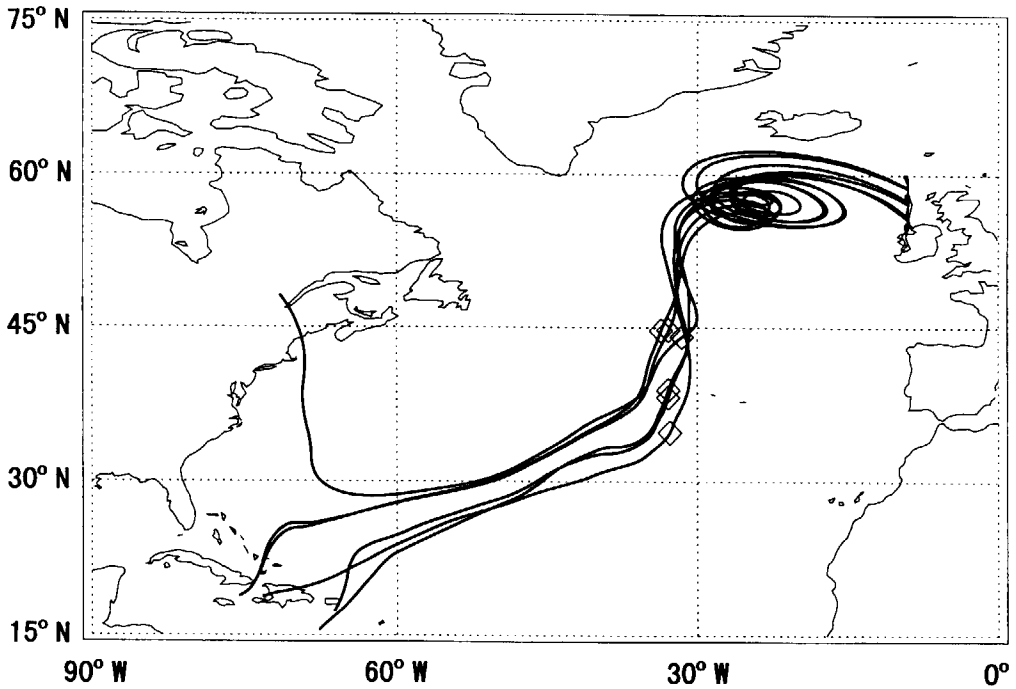
75° N
60° N
45° N
30° N
15° N
90° W
60° W
30° W
0°

Fig. 11

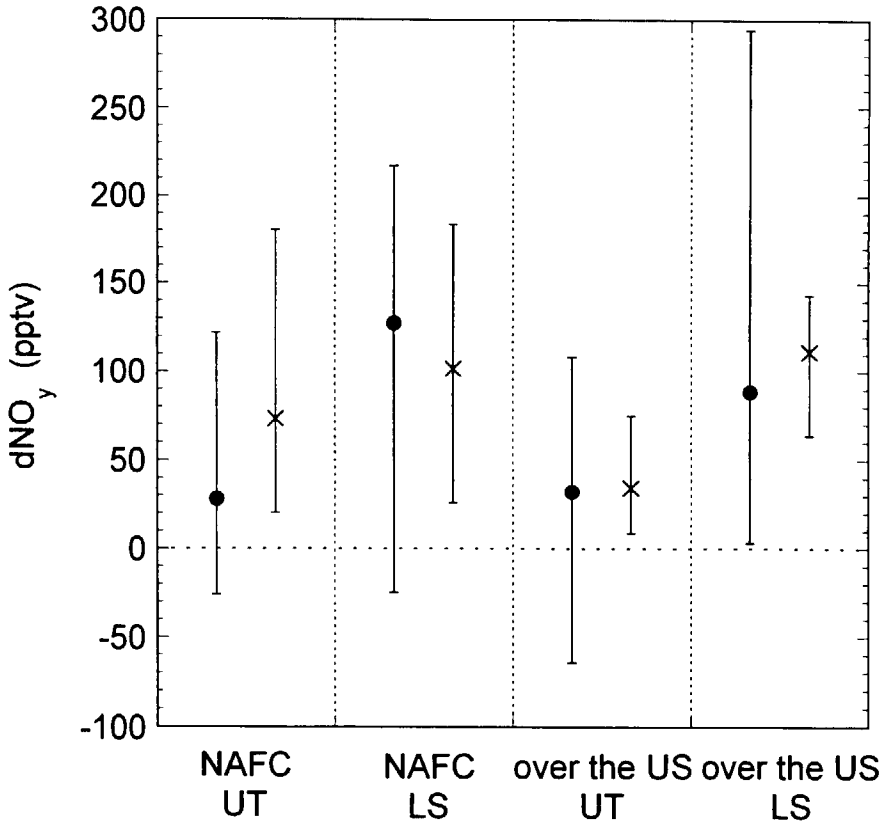
300
250
200
150
100
50
0
-50
-100
dNO$_y$ (pptv)
NAFC UT
NAFC LS
over the US UT
over the US LS

Fig. 12

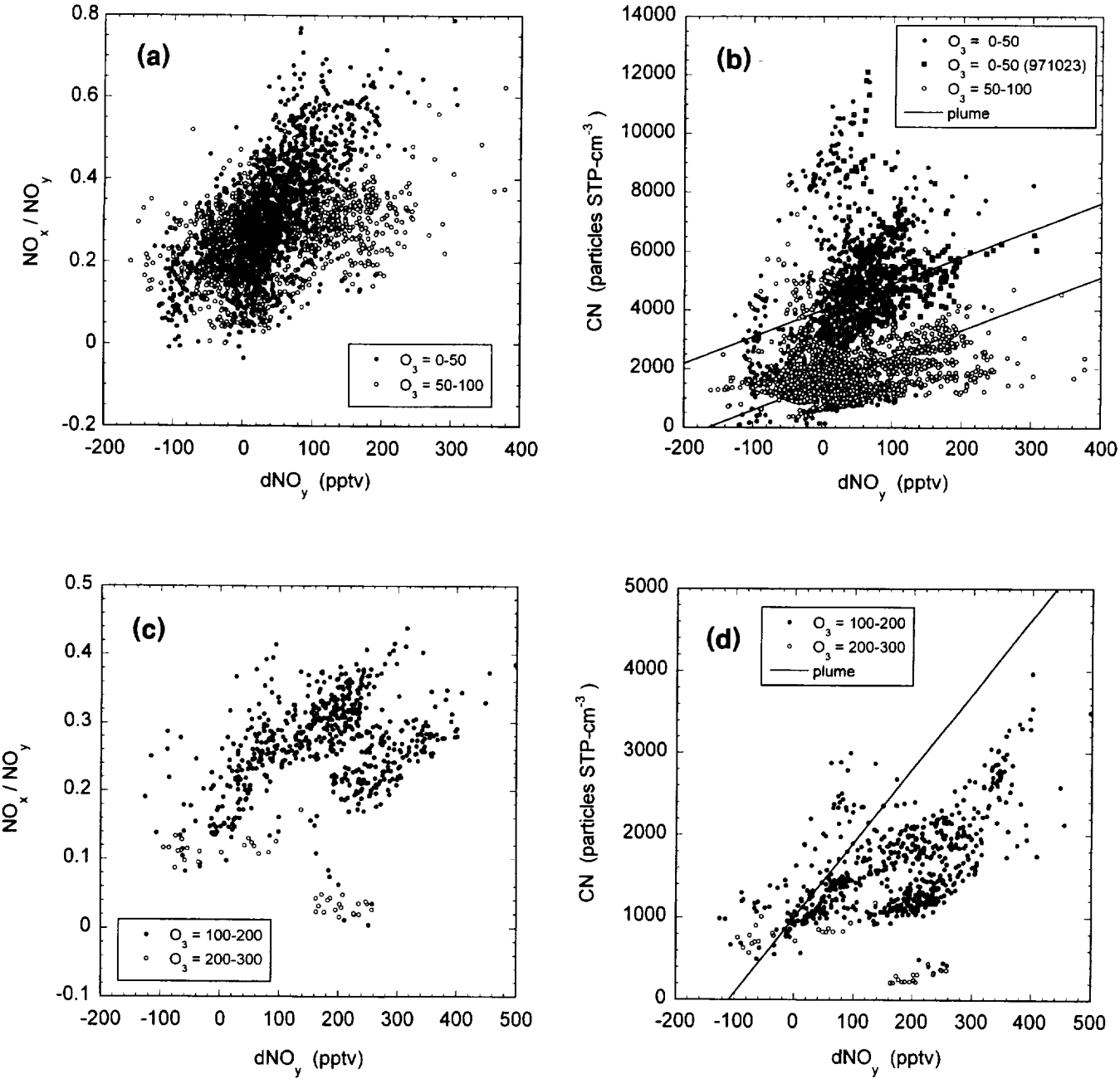
(a)
NO_x / NO_y
dNO_y (pptv)
O_3 = 0-50
O_3 = 50-100
(b)
CN (particles STP-cm^{-3})
dNO_y (pptv)
O_3 = 0-50
O_3 = 0-50 (971023)
O_3 = 50-100
plume
(c)
NO_x / NO_y
dNO_y (pptv)
O_3 = 100-200
O_3 = 200-300
(d)
CN (particles STP-cm^{-3})
dNO_y (pptv)
O_3 = 100-200
O_3 = 200-300
plume

Fig 13

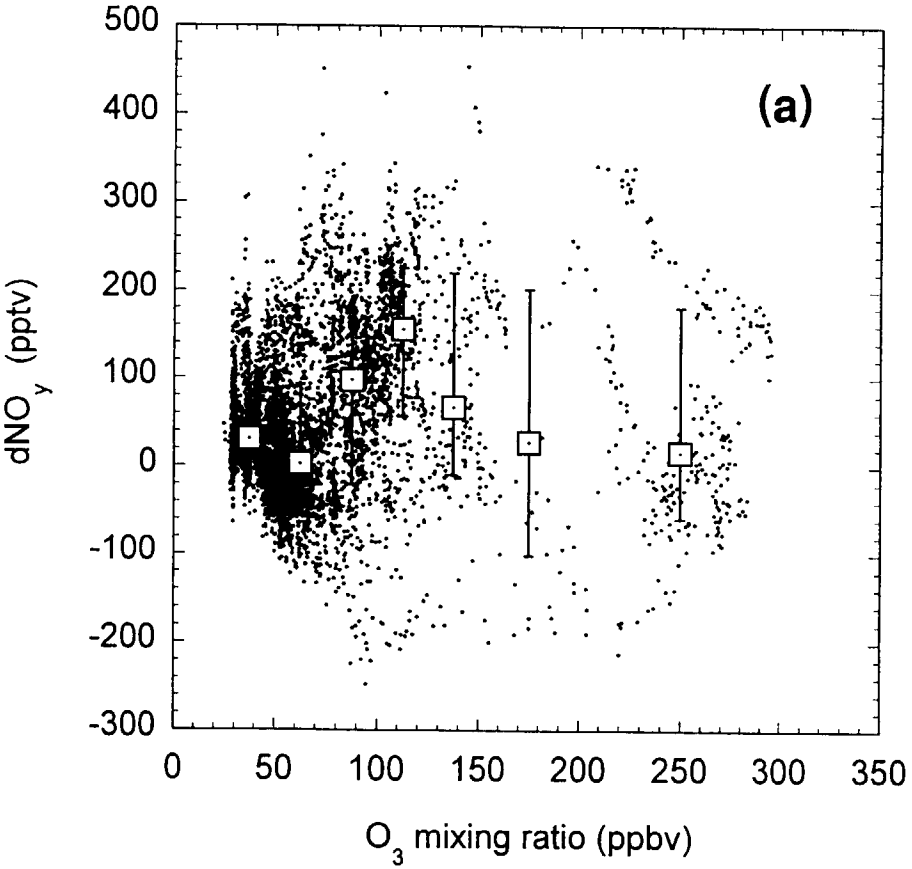
(a)
dNO$_y$ (pptv)
500
400
300
200
100
0
-100
-200
-300
0
50
100
150
200
250
300
350
O$_3$ mixing ratio (ppbv)

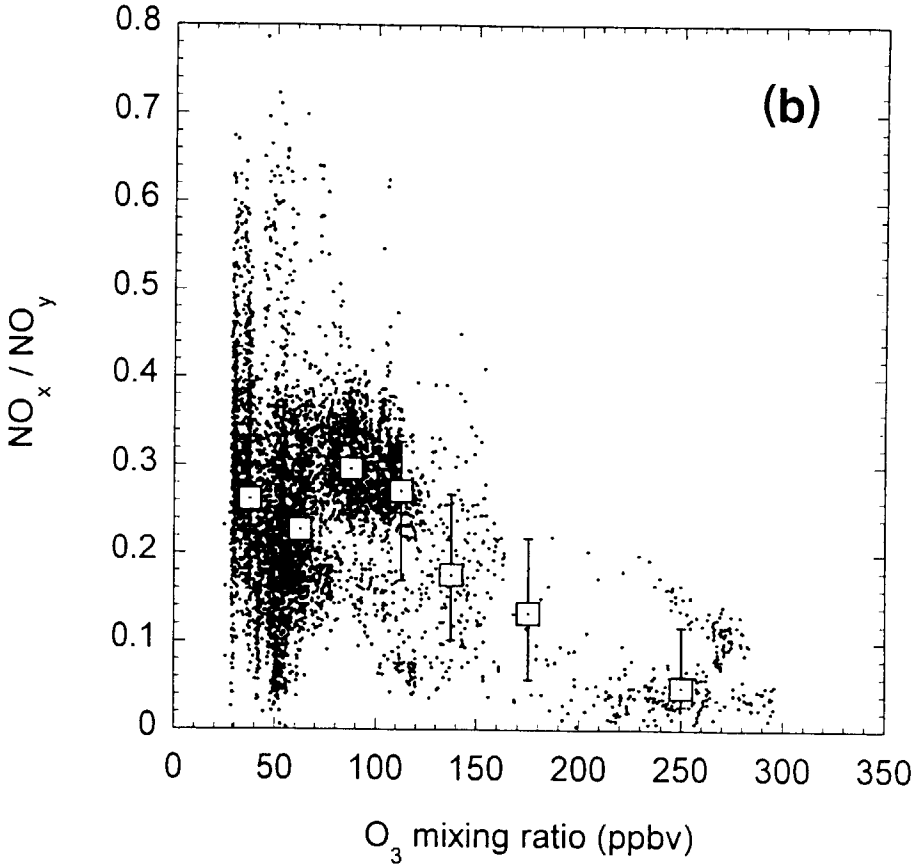
(b)
NO$_x$ / NO$_y$
0.8
0.7
0.6
0.5
0.4
0.3
0.2
0.1
0
0
50
100
150
200
250
300
350
O$_3$ mixing ratio (ppbv)

Plate 2

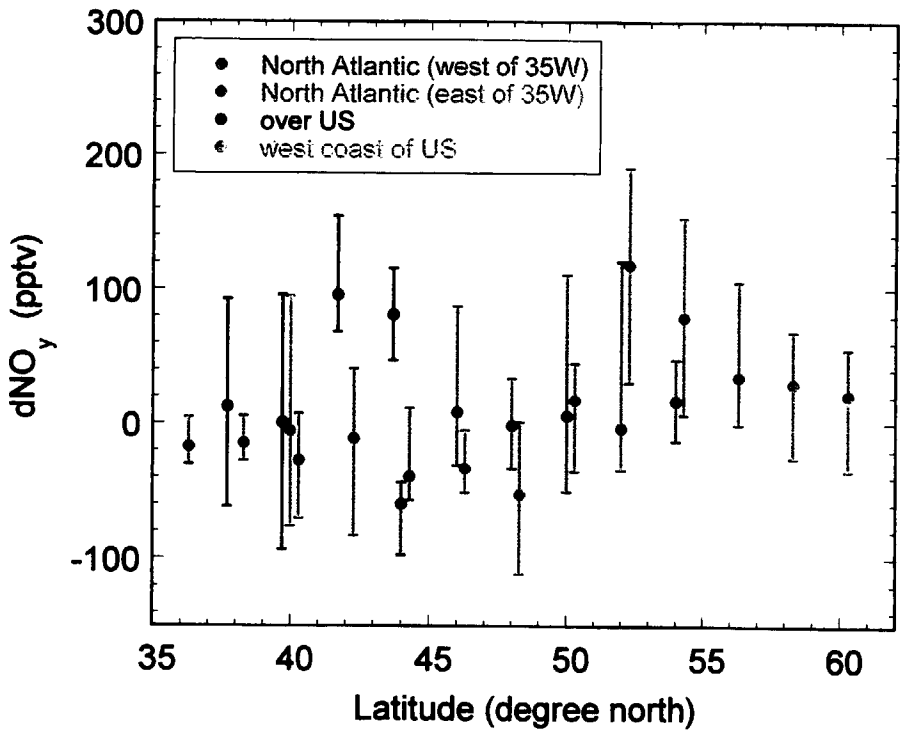

Fig. 14